Article

mTORC1 signaling in group 2 innate lymphoid cells coordinates neuro-immune crosstalk in allergic lung inflammation

Check for updates

Dongdi Wang[1,2,3,8], Lin Hu[1,2,3,8], Jinyu Chen[1,2,3], Jinxin Qiu[4], Yue Chen[4], Michelle Zhang[2], Linfeng Zhao[1,2,3], Xiaohui Su[1,2,3], Jiping Sun[1,2,3], Ju Qiu [4], Wei Tang [1,5] ✉, Wenyong Zhou [6] ✉ & Lei Shen [1,2,3,7] ✉

Group 2 innate lymphoid cells (ILC2) initiate pathologic type 2 inflammation in allergic asthma in response to diverse tissue-derived stimuli. However, the molecular mechanisms by which ILC2 cells integrate and respond to environmental signals are unclear. Here, we show in a mouse model that in allergic asthma, mechanistic target of rapamycin complex 1 (mTORC1) activation in lung ILC2 cells increases. Genetic ablation of Raptor, an obligatory component of mTORC1 complex, results in reduced IL-5 and IL-13 production in ILC2 cells and protects mice from allergic inflammation. Pharmacological inhibition of mTORC1 by rapamycin suppresses ILC2 activation and ameliorates allergic lung inflammation. Mechanistically, mTORC1 activation upregulates neuromedin U receptor 1 (NMUR1) expression through epigenetic reprogramming, which augments ILC2 activation in response to neuromedin U (NMU). However, our experiments suggest that NMUR1 is not an exclusive mediator of ILC2 activation downstream of mTORC1. In conclusion, our work reveals that in ILC2s, mTORC1 signaling coordinates neuro-immune crosstalk for optimal activation, and highlights mTORC1 as a potential therapeutic target for allergic asthma.

Allergic asthma is an increasingly prevalent chronic inflammatory airway disease characterized by type 2 inflammation[1]. Although Th2 cells are classically considered to play an essential role in the pathogenesis of asthma[2], recent studies indicate that group 2 innate lymphoid cells (ILC2) have emerged as key initiators of allergic airway inflammation[3–5].

As tissue-resident lymphocytes, ILC2s interact with epithelial cells, neurons, and other immune cells within the tissue environment to regulate tissue homeostasis and inflammation[6,7]. During allergic asthma, damaged epithelial cells release alarmin cytokines, including interleukin-25 (IL-25), IL-33, and thymic stromal lymphopoietin (TSLP)[8–10]. Neurons sense alarmins and produce neurotransmitters and neuropeptides, such as neuromedin U (NMU), calcitonin gene-related peptide (CGRP), acetylcholine (Ach), and norepinephrine (NE)[11–20]. ILC2s directly respond to these tissue-derived stimuli and produce type 2 cytokines, leading to smooth muscle contraction, eosinophil infiltration, and goblet cell hyperplasia[6,7,10,21–24]. Given that ILC2s can

[1]Center for Immune-Related Diseases at Shanghai Institute of Immunology, Ruijin Hospital, Shanghai Jiao Tong University School of Medicine, Shanghai, China. [2]Department of Immunology and Microbiology, Key Laboratory of Cell Differentiation and Apoptosis of Chinese Ministry of Education, Shanghai Jiao Tong University School of Medicine, Shanghai, China. [3]Shanghai Key Laboratory of Tumor Microenvironment and Inflammation, Shanghai Jiao Tong University School of Medicine, Shanghai, China. [4]CAS Key Laboratory of Tissue Microenvironment and Tumor, Shanghai Institute of Nutrition and Health, University of Chinese Academy of Sciences, Chinese Academy of Sciences, Shanghai, China. [5]Department of Pulmonary and Critical Care Medicine, Ruijin Hospital, Shanghai Jiao Tong University School of Medicine, Shanghai, China. [6]Department of Thoracic Surgery, Shanghai Chest Hospital, Shanghai Jiao Tong University, Shanghai, China. [7]Hainan Academy of Medical Sciences, Hainan Medical University, Hainan, China. [8]These authors contributed equally: Dongdi Wang, Lin Hu. ✉e-mail: tina_tangwei@163.com; zhou.wenyong@shsmu.edu.cn; lshen@shsmu.edu.cn

perceive multiple signals, identifying the molecular mechanisms by which ILC2s integrate and respond to the environmental cues during asthma is an important question.

Through mining RNA sequencing (RNA-seq), we found that lung ILC2s from papain-challenged mice exhibited enhanced activation of the mechanistic target of rapamycin Complex 1 (mTORC1) signaling pathway. mTORC1 acts as a central hub for sensing and integrating diverse environmental signals, including growth factors, cytokines, nutrients, and hormones, to regulate cellular metabolism, growth, and function[25–33]. Previous studies have shown that mTORC1 can mediate ILC2 activation in response to IL-33, amino acids, and glucose[34–36]. However, how mTORC1 coordinates the diverse tissue signals in the lung ILC2s during allergic asthma, and what are the molecular links that mTORC1 connects cell metabolism and ILC2 effector function, remain unknown.

Here, we identify mTORC1 as a key regulator that governs lung ILC2 activation in allergic asthma. mTORC1 promotes neuromedin U receptor 1 (NMUR1) expression level to amplify ILC2 activation in response to NMU. The expression of NMUR1 is regulated through metabolite-mediated histone acetylation. Therefore, inhibition of mTORC1 or histone acetylation suppresses ILC2 activation and ameliorates allergic lung inflammation.

Results

mTORC1 is activated in lung ILC2s during allergic inflammation
Lung ILC2s sense various environmental stimuli and rapidly produce type 2 cytokines to initiate allergic airway inflammation[3,21,23,37,38] (Supplementary Fig. 1a–e). To identify the molecular mechanisms responsible for ILC2 pathogenic activation during allergic inflammation, we performed bulk RNA sequencing (RNA-seq) of lung ILC2s sorted from wild-type (WT) or protease allergen papain-treated mice. Gene Ontology (GO) analysis showed that ILC2s from asthmatic mice were characterized by the enrichment of pathways associated with metabolic processes in addition to lymphocyte activation and inflammatory response (Fig. 1a). Heatmap confirmed that genes associated with ILC2 activation and effector function were highly expressed in papain-treated mice (Supplementary Fig. 1f). To investigate the regulatory mechanisms of cellular metabolism in activated lung ILC2s, we performed Ingenuity pathway analysis (IPA) and identified Raptor (encoded by gene Rptor) and mTOR as the top upstream metabolic regulators (Fig. 1b). In line with the above data, Gene Set Enrichment Analysis (GSEA) revealed that mTORC1 signaling pathway was enriched in activated ILC2s from asthmatic mice (Fig. 1c). The activation of mTORC1 in lung ILC2s was confirmed by Immunoblotting detecting the phosphorylation of S6 (p-S6), 4EBP1 (pE-BP1) and Raptor (p-Raptor)[39,40] (Fig. 1d–f). Interestingly, both IL-33 and IL-25 induced mTORC1 activation in ILC2 (Supplementary Fig. 1g). We further delineate the dynamics of mTORC1 activation and lung ILC2 activation during papain-induced allergic inflammation. Notably, mTORC1 activation was detected as early as 8 hours after papain treatment (Fig. 1g, h). However, the increase in type 2 cytokine production and activation marker expression in ILC2s was not observed until 24 hours post-treatment (Fig. 1i, j and Supplementary Figs. 1h, 2a, b). The increase in the frequency and number of ILC2s and eosinophils was observed on day 3 (Fig. 1k, l). mTORC1 activation occurred prior to ILC2 activation and expansion, suggesting that mTORC1 might control ILC2 activation during allergic inflammation.

Ablation of Raptor in ILC2s ameliorates allergic asthma
ILC2s are the predominant cells for IL-5 production in the lung, and Il5RFP-cre (R5/+) mice have been used for selective deletion of genes in ILC2s[22]. To determine the impact of mTORC1 on ILC2 activation, we generated Il5RFP-cre (R5/+) Rptor[f/f] mice (R5/+ Rptor[f/f]) to delete Raptor, an adapter protein of the mTORC1 complex, in ILC2s[39] (Supplementary Fig. 3a, b). The efficiency of Rptor depletion in ILC2s exceeded

70% as shown by quantitative real-time PCR (qRT–PCR) (Supplementary Fig. 3c). The reduced mTORC1 activity was confirmed by flow cytometry and Immunoblotting, which showed a significant decrease in phosphorylation of S6 and 4E-BP1 in R5/+ Rptor[f/f] ILC2s (Supplementary Fig. 3d–f). Under steady state, the frequency, cell number, and activation state of lung ILC2s were unaffected in R5/+ Rptor[f/f] mice (Supplementary Fig. 3g, h). However, R5/+ Rptor[f/f] mice exhibited a dramatic decrease in IL-5 and IL-13 production by ILC2s compared to R5/+ control mice (Fig. 2a–d and Supplementary Fig. 2b). Collectively, these results indicate that mTORC1 is required for maintaining lung tissue ILC2 homeostasis. Unlike lung ILC2s, Raptor deficiency led to a decrease of both cell number and cytokine production in ILC2s from large intestine and adipose tissue, indicating a tissue-specific role of mTORC1 in regulating ILC2s (Supplementary Figs. 2b–d and 3i, j).

Given the essential role of ILC2s in the initiation of type 2 inflammation, we next determined whether mTORC1 regulates ILC2-mediated allergic lung inflammation. Both R5/+ and R5/+ Rptor[f/f] mice were challenged with the protease allergen papain to induce acute lung allergic inflammation. Compared with R5/+ control mice, R5/+ Rptor[f/f] mice exhibited a marked decrease in the frequency and number of ILC2s (Fig. 2e, f). To investigate the mechanisms responsible for the impaired ILC2 expansion in R5/+ Rptor[f/f] mice, we examined cell proliferation by Ki67 staining and apoptosis by the expression of active caspase 3. We found that Ki67+ ILC2s decreased dramatically, whereas the expression of active caspase 3 was not affected in R5/+ Rptor[f/f] mice (Fig. 2g, h and Supplementary Fig. 3k). In addition, Raptor deletion resulted in diminished IL-5 and IL-13 production and reduced expression of activation markers in ILC2s (Fig. 2i–l and Supplementary Fig. 3l). Consistently, the levels of IL-5 and IL-13 in bronchoalveolar lavage fluid (BALF) from R5/+ Rptor[f/f] mice were significantly reduced as well (Fig. 2m). In line with the decreased ILC2 responses, R5/+ Rptor[f/f] mice showed reduced infiltration of eosinophils in both BALF and lung tissue (Fig. 2n, o and Supplementary Fig. 2e) and remission of lung inflammation as indicated by Alcian Blue–Periodic Acid–Schiff (AB-PAS) and hematoxylin-eosin (H&E) staining (Fig. 2p and Supplementary Fig. 3m).

To further corroborate the function of mTORC1 in ILC2s and allergic inflammation, we challenged R5/+ Rptor[f/f] mice and control R5/+ mice with the Alternaria alternata extract[41], a fungal allergen associated with severe asthma in humans (Supplementary Fig. 4a). Consistent with the observations in the papain-induced inflammatory model, the frequency and number of ILC2s in the lungs, the expression of IL-5 and IL-13, as well as eosinophil infiltration and mucus production were all decreased in R5/+ Rptor[f/f] mice (Supplementary Fig. 4b–g). We also investigated the effect of mTORC1 in ILC2s using a house dust mite (HDM), another clinically relevant allergen, -driven asthma model[12] (Supplementary Fig. 5a). Similar to the findings from papain- and Alternaria alternata-induced models, R5/+ Rptor[f/f] mice exhibited less ILC2 numbers, diminished type 2 cytokine production, reduced eosinophil infiltration and mucus production in the lung compared to control mice (Supplementary Fig. 5b–g). We also analyzed Th2 responses in the HDM-induced model. As expected, Th2 responses were not affected in R5/+ Rptor[f/f] mice (Supplementary Fig. 5h–k). This might be explained by ILC2s were the predominant IL-5+ cells in R5/+ Rptor[f/f] mice (Supplementary Fig. 5l). Together, these data suggest that mTORC1 is required for ILC2 pathogenic activation during allergic inflammation.

mTORC1 regulates lung ILC2 function in a cell-intrinsic manner
Given that NMUR1 was specifically expressed on ILC2s in the lung[13,14,18,42] (Supplementary Fig. 6a–c), we employed Nmur1[iCre-TdT] Rptor[f/f] mice to specifically delete Raptor in ILC2s. The deletion efficiency of Rptor in ILC2s was confirmed (Supplementary Fig. 7a). Under steady state, Nmur1[iCre-TdT] Rptor[f/f] mice had no change in ILC2 number and activation, but had less IL-5 and IL-13 production (Supplementary
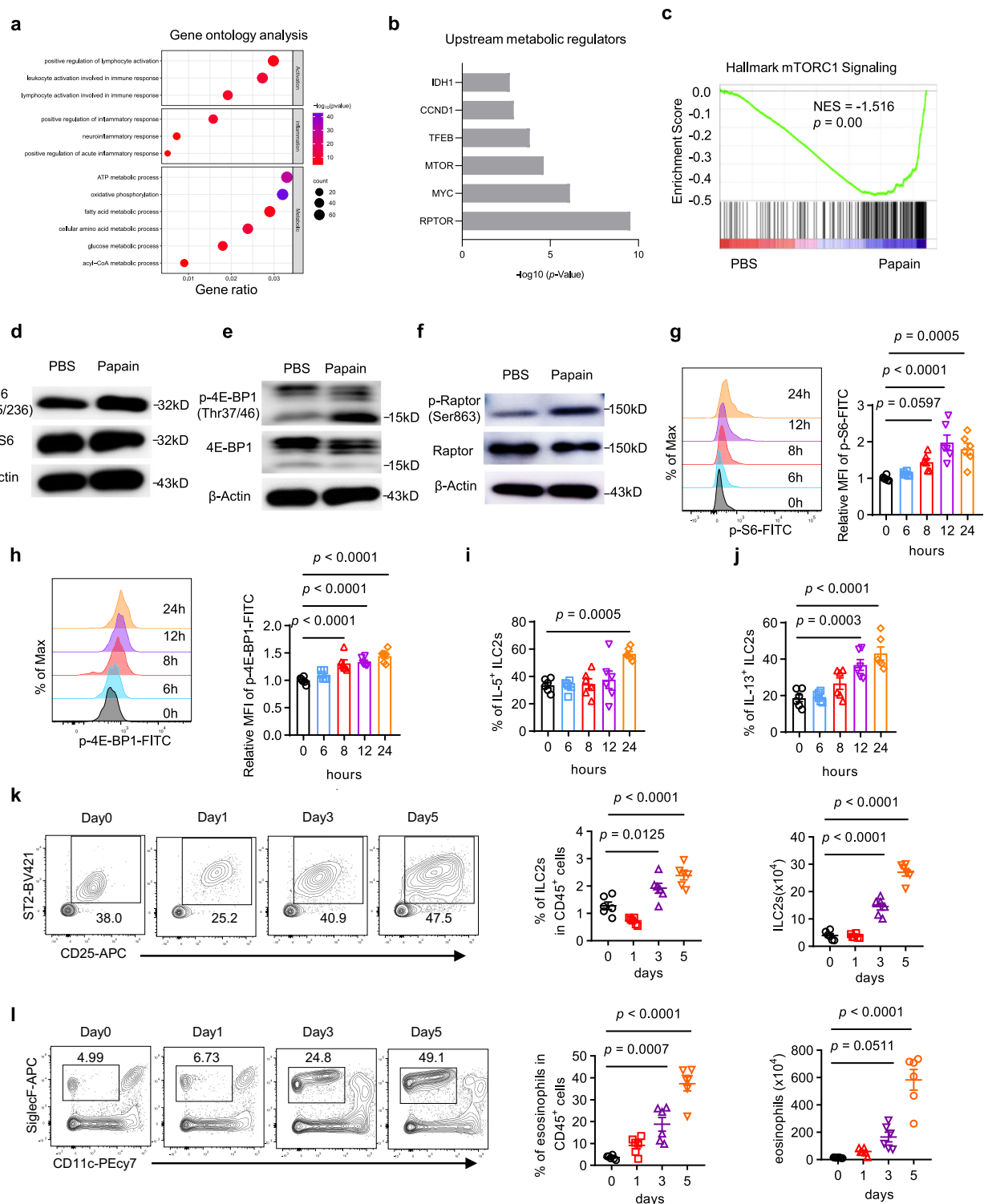
Fig. 7b–e). Upon papain challenge, *Nmur1*^iCre-TdT *Rptor*^f/f mice exhibited decreased ILC2 cell number (Fig. 3a and Supplementary Fig. 7f), diminished type 2 cytokine production (Fig. 3b, c), reduced eosinophil infiltration (Fig. 3d), and less mucus production in the lung (Fig. 3e and Supplementary Fig. 7g). To further confirm the cell-intrinsic role of mTORC1 in regulating ILC2 function and allergic inflammation, lung ILC2s sorted from R5/+(referred as control) or R5/+ *Rptor*^f/f (referred as KO) mice were transferred to *Rag2*^−/−*Il2rg*^−/− mice, which were followed by intranasal administration of papain to induce allergic asthma. Both control and KO ILC2s reconstituted successfully in the lung of recipient mice (Supplementary Fig. 8a). After papain challenge, we

observed less ILC2s infiltrated in the lung of mice that received KO ILC2s, which was due to the impaired cell proliferation as indicated by the decreased percentage of Ki67⁺ ILC2 cells (Fig. 3f and Supplementary Fig. 8b). In addition, a significant decrease in IL-13 and IL-5 production was observed in KO ILC2s (Fig. 3g and Supplementary Fig. 8c). In line with the cellular data, mice that received KO ILC2s displayed reduced lung inflammation, as indicated by reduced eosinophil infiltration in the lung and less mucin production in AB-PAS staining (Fig. 3h, i and Supplementary Fig. 8d). These data support the notion that Raptor acts in a cell-autonomous manner in regulating the function of lung ILC2s in allergic asthma.

Fig. 1 | mTORC1 is activated in lung ILC2s during allergic inflammation.
a–**c** RNA-seq analysis of sorted ILC2s from PBS- or papain-treated C57BL/6 wild-type mice ($n = 3$). **a** Gene ontology (GO) analysis of genes upregulated in papain-treated ILC2s. **b** Top upstream metabolic regulators of differentially regulated proteins between papain- and PBS-treated ILC2s were identified using Ingenuity Pathway Analysis (p-value < 0.05, fold change > 1.5), with significance determined by the method implemented in software. **c** Gene set enrichment analysis (GSEA) was performed using the webtool from Broad Institute. NES, normalized enrichment score. Significance was determined by the method implemented in the software (nominal p < 0.05). **d**–**f** Wild-type mice were challenged with papain intranasally to induce asthma. Lung tissues were collected on day 6, and ILC2s were sorted for western blot analysis. The experiments were repeated two times with similar results, and the representative immunoblot images were shown.

d Phosphorylated S6 (p-S6) and total S6 expression by western blot.
e Phosphorylated 4E-BP1 (p-4E-BP1) and total 4E-BP1 expression by western blot.
f Phosphorylated Raptor (p-Raptor) and total Raptor expression by western blot.
g–**l** Wild-type mice were challenged with papain intranasally. Lung tissues were collected at the indicated time points. g, Relative mean fluorescence intensity (MFI) of p-S6 in ILC2s by flow cytometry ($n = 6$). h, Relative MFI of p-4E-BP1 in ILC2s by flow cytometry ($n = 6$). **i**, **j** Frequency of IL-5$^+$ (**i**) and IL-13$^+$ (**j**) ILC2s ($n = 6$). **k**, **l** Frequency and absolute counts of ILC2s (**k**) and eosinophils (**l**) in the lung ($n = 5$). Each symbol represents an individual mouse (**g**–**l**). Data were pooled from two independent experiments (**g**–**l**) and are presented as mean ± SEM. Statistical analysis was determined by one-way analysis of variance (ANOVA) in (**g**–**l**). p-values are shown on the graphs, and p-values < 0.0001 are reported as such. Source data are provided as a Source Data file.

mTORC1 regulates NMUR1 expression on ILC2s

To investigate the molecular mechanisms of mTORC1 regulating the function of lung ILC2s, we performed RNA-seq analysis to compare the global transcriptomes of lung ILC2s sorted from R5/+(referred as control) or R5/+ *Rptor*$^{f/f}$ (referred as KO) mice. A total of 3059 transcripts were differentially expressed (fold change > 1.2, P < 0.05) between control and KO ILC2s. Among these genes, 1571 genes were upregulated and 1488 genes were down-regulated in KO ILC2 (Supplementary Fig. 9a). GO analysis revealed that genes that were decreased in KO ILC2s were enriched in pathways associated with cell surface receptor signaling and glucose metabolism, in addition to lymphocyte activation, which were consistent with the changes in activated ILC2s from papain-induced asthmatic mice (Fig. 4a). By analyzing the expression profile of genes encoding activating receptors on ILC2s, we found that *Nmur1*, encoding the receptor for NMU, was downregulated significantly in KO ILC2s (Fig. 4b, c). The reduced expression of NMUR1 in KO ILC2s was confirmed by detecting the protein level using immunofluorescence and flow cytometry (Fig. 4d, e). To further corroborate the downregulation of NMUR1, we employed *Nmur1*$^{iCre-TdT}$ *Rptor*$^{f/f}$ mice, in which Raptor was specifically deleted in ILC2s and the expression of NMUR1 was represented by the tomato reporter. Similar to the findings in R5/+ *Rptor*$^{f/f}$ mice, the expression of NMUR1 in *Nmur1*$^{iCre-TdT}$ *Rptor*$^{f/f}$ lung ILC2s was decreased significantly (Supplementary Fig. 9b). Not only in the lung, *Nmur1*$^{iCre-TdT}$ *Rptor*$^{f/f}$ ILC2s in other tissues, including the small intestine, large intestine and adipose tissue, also displayed diminished NMUR1 expression (Supplementary Fig. 9c–f). Consistently, we observed that rapamycin suppressed NMUR1 expression on ILC2s cultured in vitro (Supplementary Fig. 9g, h). Together, these data suggest that mTORC1 regulates NMUR1 expression on ILC2s.

The reduced NMUR1 expression prompted us to speculate that Raptor-deficient ILC2s are defective in response to NMU stimulation. To test this hypothesis, both control and KO ILC2 were stimulated with NMU in vitro in the presence of IL-7. As expected, KO ILC2s produced less IL-5, IL-13 compared to control ILC2s (Fig. 4f, g and Supplementary Fig. 9i, j). Next, we examined ILC2 responses by administering NMU intranasally to both R5/+ or R5/+ *Rptor*$^{f/f}$ mice. R5/+ *Rptor*$^{f/f}$ mice exhibited less ILC2 expansion and reduced type 2 cytokine production (Fig. 4h–j). Consistently, we observed reduced lung inflammation in R5/+ *Rptor*$^{f/f}$ mice, as indicated by less eosinophil infiltration and less mucin production (Fig. 4k, l and Supplementary Fig. 9k). These data suggest that mTORC1 determines the magnitude of the ILC2 response to NMU.

To rule out the possibility that NMU-induced ILC2 activation is dependent on mTORC1, we examined mTORC1 activation in cultured ILC2s upon NMU stimulation. The phosphorylation of S6 and 4E-BP1 in ILC2s was not affected by NMU (Supplementary Fig. 9l, m). In line with these data, NMU did not increase mTORC1 activation induced by IL-33. Hence, the synergistic effect of NMU and IL-33 on ILC2 effector function was not attributable to mTORC1 activation (Supplementary Fig. 9n, o). Given that NMU-induced activation of

Ca^{2+}–calcineurin–NFAT and ERK1/2 pathways[13], it is likely that NMU and IL-33 engage distinct signaling cascades that converge to cooperatively enhance ILC2 effector functions.

mTORC1 promotes ILC2 activation partly through upregulation of NMUR1

We next investigated whether decreased ILC2 response in KO ILC2s is caused by reduced NMUR1 expression. Overexpression of NMUR1 by retroviral gene transfer successfully restored NMUR1 expression and IL-5 and IL-13 production in Raptor-deficient ILC2s stimulated with NMU in vitro (Fig. 5a, b and Supplementary Fig. 10a, b). Since both NMU and NMUR1 were increased significantly in the lung tissue of papain-treated mice (Fig. 5c–e), we hypothesized that mTORC1 regulating ILC2 activation in allergic asthma was dependent on the NMU/NMUR1 axis. To test this hypothesis, Raptor-deficient ILC2s expressing NMUR1 were transferred to *Rag2*$^{-/-}$*Il2rg*$^{-/-}$ mice, which were followed by intranasal administration of papain to induce allergic asthma. Compared to the mice receiving KO ILC2s, mice receiving KO ILC2s expressing NMUR1 exhibited a significant increase in cell numbers and type 2 cytokine production (Fig. 5f–h). However, these responses were not fully restored to the levels observed in mice receiving control ILC2s (Fig. 5f–h). Consistently, overexpression of NMUR1 in KO ILC2s partially restored allergic inflammation in the lung, as indicated by increased eosinophil infiltration and mucus production (Fig. 5i, j). Together, these data suggest that mTORC1 promotes ILC2 activation in allergic asthma partly through upregulation of NMUR1. Given that NMU was mainly expressed in neurons[13,14,18,43,44], and lung ILC2s were distributed in the vicinity of local neurons (Supplementary Fig. 10c), the regulation of mTORC1 on ILC2 activation is presumably mediated through ILC2–neuronal interactions.

mTORC1 induces NMUR1 expression through an epigenetic mechanism

Next, we sought to address how mTORC1 regulates NMUR1 expression. RNA-seq data have shown that Raptor deficiency led to impaired glucose metabolism (Fig. 4a), which were consistent with the changes in activated ILC2s from papain-induced asthmatic mice. To validate the transcriptional changes of the cellular metabolism in KO ILC2s, we performed Seahorse metabolic assays to measure extracellular acidification rate (ECAR) and oxygen consumption rate (OCR). Raptor deletion led to a reduction in both glycolysis and glycolytic reserve, as well as a decrease in basal respiration and maximal respiratory capacity (Fig. 6a, b). In line with the reduction in glucose metabolism, KO ILC2s exhibited decreased glucose uptake (Fig. 6c). Lipid uptake was also decreased (Supplementary Fig. 10d). Recent studies indicate that glucose metabolism is involved in regulating gene expression through epigenetic mechanisms including histone acetylation[45–47]. To determine whether NMUR1 expression is regulated by histone acetylation in KO ILC2s, we first analyzed the levels of histone H3 acetylation at the lysine 9 (H3K9Ac) and
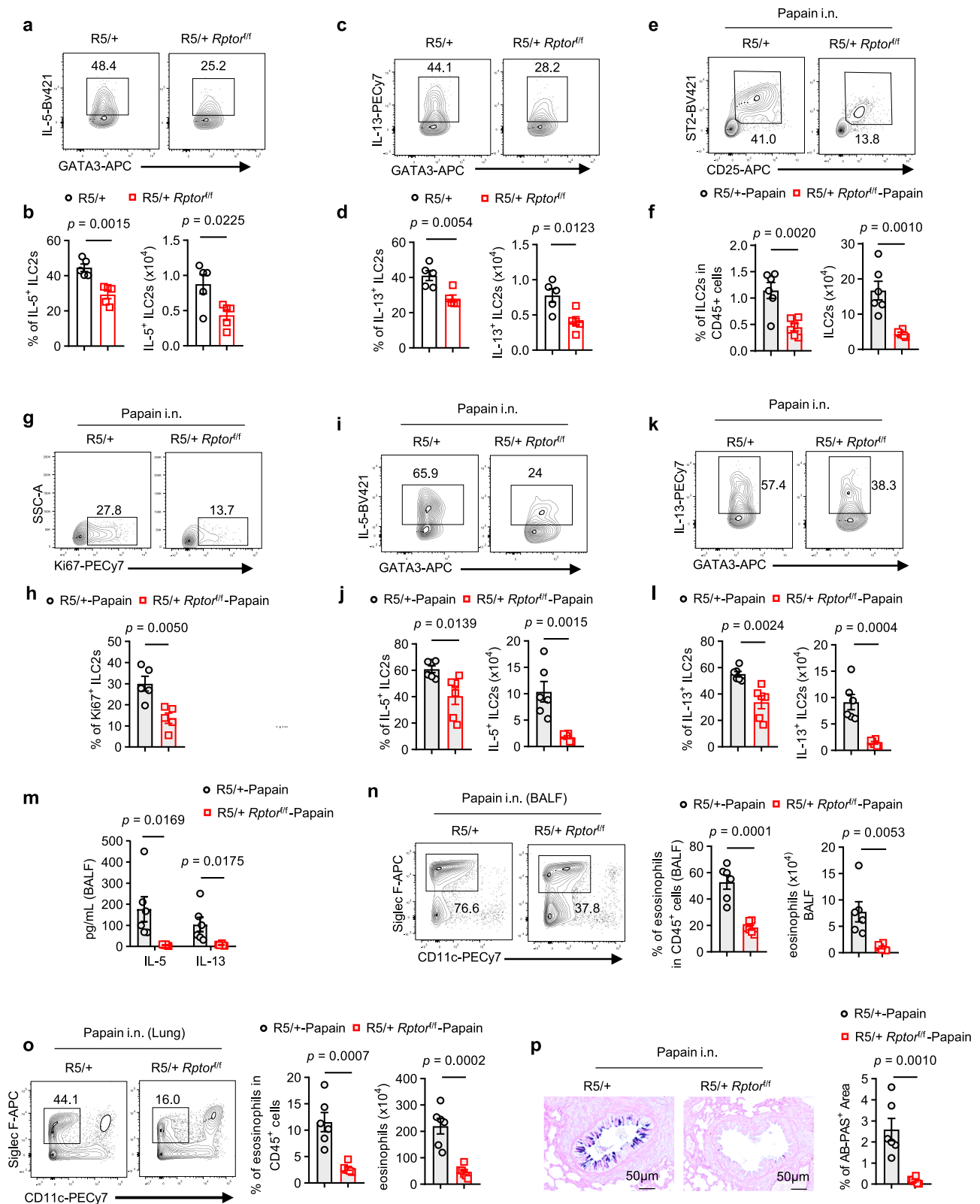
Fig. 2 | Ablation of Raptor in ILC2s ameliorates allergic asthma. a–d Frequency and total number of IL-5$^+$ ILC2s (a,b) and IL-13$^+$ ILC2s (**c, d**) in the lung of R5/+ and R5/+ *Rptor*$^{f/f}$ (KO) mice (*n* = 5). Cells were gated on CD45$^+$lin$^-$CD25$^+$ST2$^+$ live cells. **e–p** R5/+ and R5/+ *Rptor*$^{f/f}$ (KO) mice were challenged with papain intranasally (i.n.). Lung tissues were collected and analyzed on day 6 (*n* = 6). **e, f** Frequency and absolute counts of lung ILC2s. **g, h** Frequency of Ki67$^+$ ILC2s (*n* = 5). **i–l** Frequency and absolute counts of IL-5$^+$ ILC2s (**i, j**) and IL-13$^+$ ILC2s (**k, l**). **m** The levels of IL-5 and IL-13 in the BALF were measured by ELISA. **n, o** Frequency and cell number of

Eosinophils (CD45$^+$CD11b$^+$Gr-1$^-$SiglecF$^+$CD11c$^-$) in bronchoalveolar lavage fluid (BALF) (**n**) and lung (**o**). **p** Paraffin-embedded lung sections were stained with Alcian Blue–Periodic Acid–Schiff (AB-PAS) and AB-PAS$^+$ (positive) area was quantified by ImageJ. Scale bars, 50 μm. Each symbol represents an individual mouse (**a–p**). Data were pooled from two independent experiments, shown as mean ± SEM. Statistical significance was determined by a two-tailed unpaired Student's *t* test in (**a–p**). *p*-values are shown on the graphs. Source data are provided as a Source Data file.
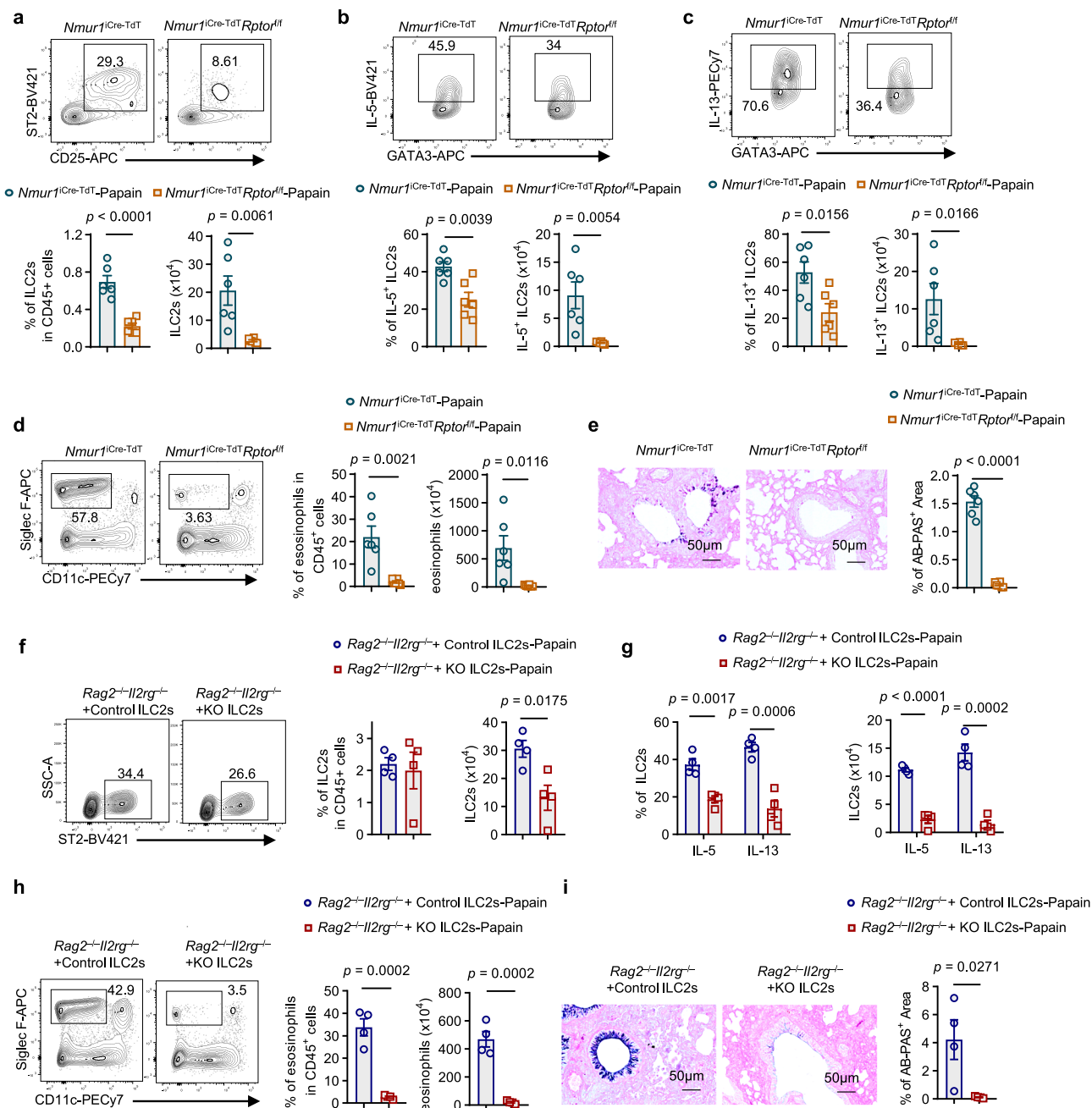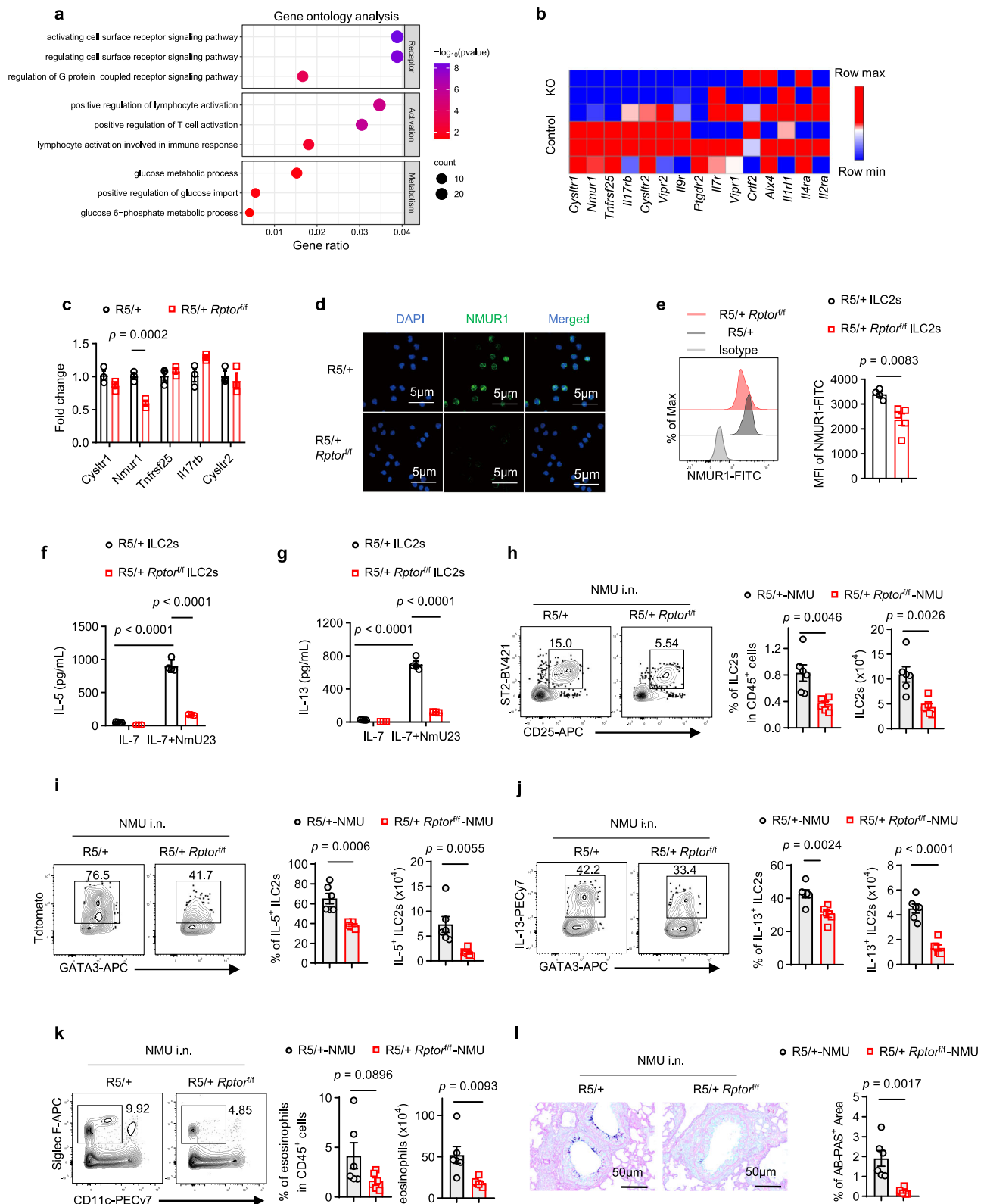
Fig. 3 | mTORC1 regulates lung ILC2 function in a cell-intrinsic manner.
a–e *Nmur1*[iCre-TdT] and *Nmur1*[iCre-TdT] *Rptor*[f/f] mice were challenged with papain. Lung tissues were collected and analyzed on day 6 (*n* = 6). **a–d** Frequency and absolute numbers of total ILC2s (**a**), IL-5⁺ ILC2s (**b**), IL-13⁺ ILC2s (**c**), and eosinophils (**d**) in the lung. **e** Representative Alcian Blue–Periodic Acid–Schiff (AB-PAS) staining of lung sections and histological quantification of AB-PAS⁺ (positive) area by ImageJ. Scale bars, 50 µm. **f–i** Lung ILC2s sorted from R5/+ (Control) or R5/+ *Rptor*[f/f] (KO) mice were transferred intravenously into *Rag2*^{−/−} *Il2rg*^{−/−} mice, which were challenged with papain subsequently. Lung tissues were collected and analyzed on day 7 (*n* = 4). **f** Frequency and absolute counts of ILC2s from recipients after ILC2 transfer. Cells were gated on CD45⁺lin⁻ live cells. **g, h** Frequency and cell number of IL-5⁺ ILC2s, IL-13⁺ ILC2s (**g**), and eosinophils (live CD45⁺GR1⁻CD11c⁻SiglecF⁺) (**h**) in the lungs. **i** Representative AB-PAS staining of lung sections and histological quantification of AB-PAS⁺ (positive) area by ImageJ. Scale bars, 50 µm. Each symbol represents an individual mouse (**a–i**). Data were pooled from two independent experiments (**a–e**), and data are representative of two (**f–i**) independent experiments shown as mean ± SEM. Statistical significance was tested by a two-tailed unpaired Student's *t* test in (**a–i**). *p*-values are shown on the graphs, and *p*-values < 0.0001 are reported as such. Source data are provided as a Source Data file.

27 (H3K27Ac) residues, which are associated with chromatin accessibility and active transcription. Both H3K9Ac and H3K27Ac were significantly decreased in Raptor-deficient ILC2s compared with control ILC2s (Fig. 6d, e). To examine the binding of H3K9Ac and H3K27Ac in the promoter region of the *Nmur1* gene, we performed chromatin immunoprecipitation–quantitative PCR (ChIP-qPCR). We found H3K27Ac was significantly reduced, but total H3 and H3K9Ac

were comparable in KO ILC2s (Fig. 6f and Supplementary Fig. 10e, f). Given that histone acetylation requires acetyl coenzyme A (acetyl-CoA) as a substrate[46,48], we hypothesized that less acetyl-CoA was generated in the cytoplasm of KO ILC2s. Indeed, we observed that total citrate, a key precursor of acetyl-CoA, and cytosolic acetyl-CoA were decreased in Raptor-deficient ILC2 cells (Fig. 6g, h). To determine whether NMUR1 expression is dependent on cytosolic

acetyl-CoA level, we inhibited ATP-citrate lyase (ACL), the enzyme converting citrate to acetyl-CoA in the cytoplasm[47], and examined NMUR1 expression in ILC2s. Interestingly, ACL inhibitor (ACLi) markedly suppressed NMUR1 expression (Fig. 6i–k). As histone acetylation requires histone acetyltransferases (HATs) to add acetyl groups from Acetyl-CoA to histones[46], we hypothesized that blockade of HAT activity would inhibit NMUR1 expression as well. Like

ACLi, HAT inhibitor (HATi) significantly suppressed NMUR1 expression in ILC2s (Fig. 6l, m). In addition, HATi treatment abolished the difference of NMUR1 expression between control and KO ILC2s, indicating that NMUR1 expression is dependent on histone acetylation (Fig. 6n). Collectively, these findings demonstrate that mTORC1 regulates NMUR1 expression through an epigenetic mechanism of histone acetylation.

Fig. 4 | mTORC1 regulates NMUR1 expression on ILC2s. a, b RNA-seq analysis of sorted ILC2s from R5/+ and R5/+ *Rptor*^f/f (KO) mice after papain treatment (*n* = 3). GO analysis of KO ILC2s downregulated genes (**a**). Heatmap of ILC2 surface receptor genes (**b**). **c** mRNA expression of ILC2 surface receptor genes (*n* = 3). **d** Immunofluorescence staining of NMUR1 (Green) in ILC2s from R5/+ and R5/+ *Rptor*^f/f mice. Scale bars, 5 μm. The experiments were repeated three times with similar results. **e** Mean fluorescence intensity (MFI) of NMUR1 in lung ILC2s from R5/+ and R5/+ *Rptor*^f/f mice (*n* = 4 for R5/+, *n* = 5 for R5/+ *Rptor*^f/f). **f, g** Sorted ILC2s from R5/+ and R5/+ *Rptor*^f/f mice were cultured with NMU (10 ng/mL) in the presence of IL-7 (10 ng/ml) for 24 h. IL-5 and IL-13 in the supernatants were detected by ELISA (*n* = 4 for R5/+, *n* = 3 for R5/+ *Rptor*^f/f). **h–l** R5/+ and R5/+ *Rptor*^f/f mice were

challenged with NMU (20 μg/30 μL/day) intranasally (i.n.) for five days. Lung tissues were collected on day 8 (*n* = 6). **h–j**, Frequency and absolute counts of total ILC2s (**h**), IL-5^+ ILC2s (**i**) and IL-13^+ ILC2s (**j**). **k** Frequency and absolute counts of eosinophils in the lungs. **l** Alcian Blue–Periodic Acid–Schiff (AB-PAS) staining of lung sections and quantification of AB-PAS^+ area by ImageJ. Scale bars, 50 μm. Each symbol represents an individual mouse (**c–l**). Data are representative of three (**c–g**) independent experiments and data were pooled from two independent experiments (**h–l**) shown as mean ± SEM. Statistical significance was determined by a two-tailed unpaired Student's *t* test (**c, e, h–l**) or two-way ANOVA followed by Tukey's multiple comparisons test in (**f, g**). *p*-values are shown on the graphs, and *p*-values < 0.0001 are reported as such. Source data are provided as a Source Data file.

Blockade of mTORC1 pathway in ILC2s ameliorates allergic asthma

Given that mTORC1 facilitated ILC2 activation and enhanced allergic airway inflammation, we hypothesized that blockade of mTORC1 could inhibit ILC2 function and improve allergic asthma. Consistent with a previous report[34,49,50], mice treated with rapamycin exhibited reduced airway inflammation, as indicated by less mucus production and eosinophil infiltration (Supplementary Fig. 11a–c). In accordance with the histology, rapamycin inhibited ILC2 expansion and type 2 cytokine production by ILC2s in the lung (Supplementary Fig. 11d–g). Notably, rapamycin also inhibited the expression of NMUR1 expression on ILC2 (Supplementary Fig. 11h). To determine whether the therapeutic effect of rapamycin blockade is dependent on ILC2s, total ILCs were depleted with anti-Thy1.2 antibody in papain-challenged *Rag1*^−/− mice[51] (Supplementary Fig. 11i). As expected, mice treated with anti-Thy1.2 antibody developed less airway inflammation than the control group of isotype-treated mice, as indicated by the reduced mucus production and eosinophil infiltration in lung, which was presumably due to the loss of ILC2s (Supplementary Fig. 11j, k). Similar to the findings in WT mice, treatment with rapamycin reduced lung inflammation compared to DMSO control in *Rag1*^−/− mice. However, the therapeutic effect of rapamycin disappeared in *Rag1*^−/− mice treated with anti-Thy1.2 antibody (Supplementary Fig. 11j, k), suggesting the efficacy of rapamycin is dependent on ILC2s. To further corroborate that mTORC1 blockade in ILC2s is responsible for the therapeutic benefits, we used *Nmur1*^iCre-TdT DTR^f/+ mice to specifically deplete ILC2s (Supplementary Fig. 11l), given that NMUR1 is specifically expressed on ILC2s[42,52]. As expected, depletion of ILC2s in *Nmur1*^iCre-TdT DTR^f/+ mice reduced eosinophil infiltration and ameliorated lung inflammation compared with control DTR^f/+ mice (Fig. 7a–c and Supplementary Fig. 11m). When treated with rapamycin, control DTR^f/+ mice displayed reduced lung inflammation (Fig. 7a–c and Supplementary Fig. 11m). However, the therapeutic effect of rapamycin disappeared in *Nmur1*^iCre-TdT DTR^f/+ mice (Fig. 7a–c and Supplementary Fig. 11m). To further confirm that inhibition of mTORC1 in ILC2s can improve asthma, rapamycin-treated ILC2s were transferred to *Rag2*^−/−*Il2rg*^−/− mice, which were subsequently challenged with papain. Mice that received rapamycin-treated ILC2s had a significant decrease in ILC2 number, type 2 cytokine production, eosinophil infiltration, and mucus production, compared with that received DMSO-treated ILC2s (Fig. 7d–l). Together, these results reveal that the therapeutic efficacy of rapamycin is dependent on ILC2s.

We further assessed the effect of HATi on ILC2 activation and allergic asthma, given that NMUR1 expression is dependent on histone acetylation and NMUR1 controls ILC2 activation magnitude. We found that HATi A-485 inhibited NMUR1 expression on ILC2s (Supplementary Fig. 12a) and suppressed ILC2 expansion and type 2 cytokine production in the lung (Supplementary Fig. 12b–d). Moreover, HATi attenuated airway inflammation, as reflected by reduced eosinophil infiltration and mucus production (Supplementary Fig. 12e, f). To determine whether the therapeutic effect of HATi is dependent on ILC2s, ILC2s treated with HATi or DMSO were transferred into *Rag2*^−/−*Il2rg*^−/− mice, followed by papain challenge. Like mice received rapamycin-treated ILC2s, recipients of HATi–treated ILC2s exhibited

decreased ILC2 number and function and reduced allergic lung inflammation (Fig. 7d–l). Together, these findings indicate that HATi ameliorates allergic asthma through inhibition of NMUR1 expression and ILC2 function.
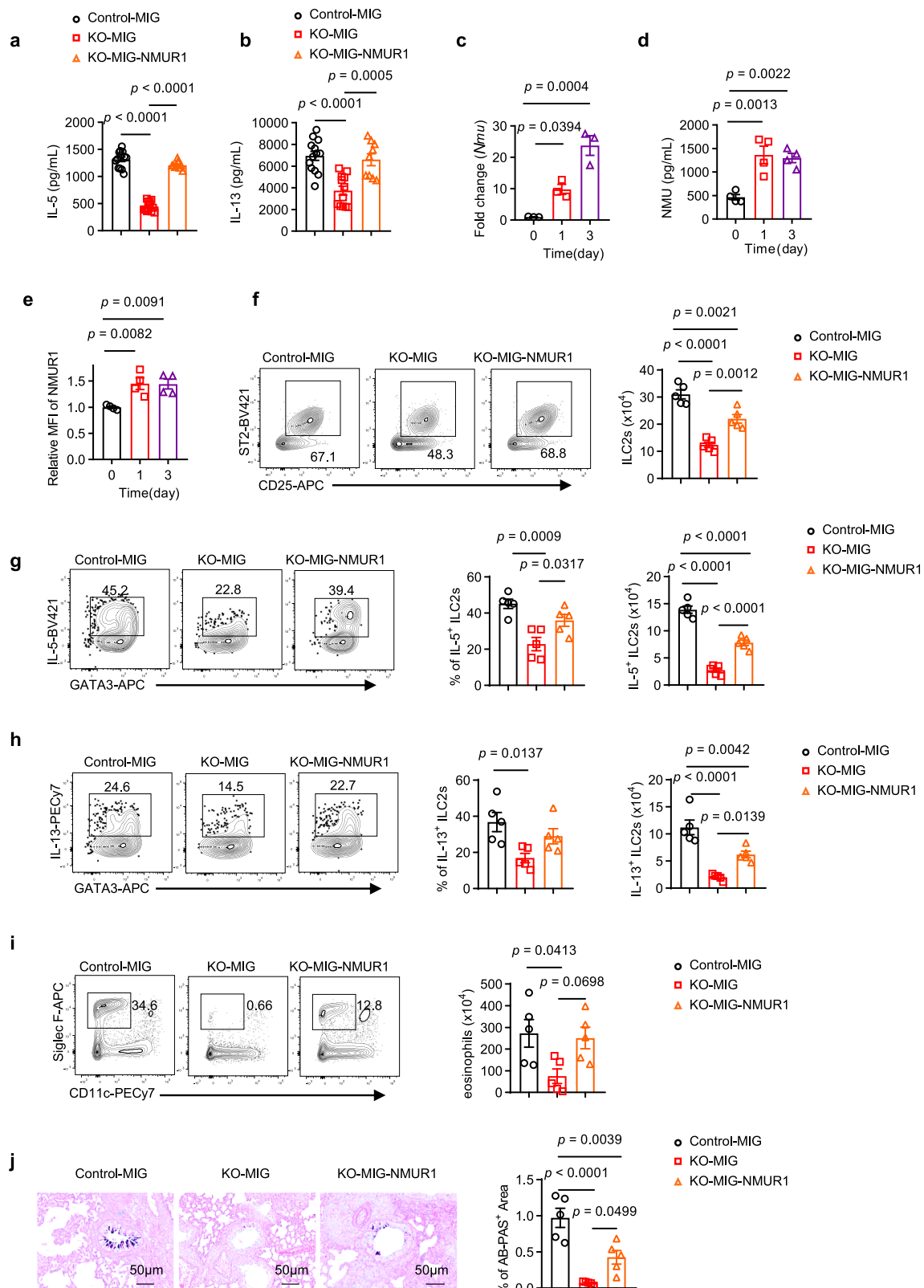
To examine whether ILC2s in asthma patients exhibit similar abnormalities as in asthmatic mice, we first analyzed ILC2s in human PBMC. In accordance with our mouse data, the frequency of ILC2s was increased in PBMC from asthma patients compared with healthy controls (Supplementary Fig. 13a, b). In addition, ILC2s from asthma patients produced more IL-5 and IL-13 (Supplementary Fig. 13c, d). Together, these data suggest that the ILC2s were activated in asthma patients. We further examined mTORC1 activation in ILC2s. Consistent with the mouse data, ILC2s from asthma patients exhibited increased mTORC1 activation and higher NMUR1 expression levels (Fig. 7m). In addition, rapamycin treatment significantly suppressed NMUR1 expression and type 2 cytokine production in human ILC2s (Fig. 7n and Supplementary Fig. 13e). Together, these findings demonstrate mTORC1 is a promising target for treating allergic inflammation.

Discussion

Lung-resident ILC2s sense and integrate various tissue-derived signals to maintain tissue homeostasis or initiate pathologic inflammation in allergic asthma[10,53]. By performing transcriptional analysis, we identify mTORC1 as a key signal pathway that is associated with pathogenic ILC2 activation in allergic asthma. Genetic deletion of Raptor or pharmacological inhibition of mTORC1 suppresses ILC2 activation and ameliorates allergic lung inflammation. Furthermore, mTORC1 regulates ILC2 glucose metabolism and induces NMUR1 expression through an epigenetic mechanism of histone acetylation. Inhibition of histone acetylation with A-485 suppresses ILC2 activation and alleviates allergic lung inflammation. As a result, mTORC1 promotes ILC2 activation by orchestrating neuro-immune interactions mediated by the NMU/NMUR1 axis. Therefore, our study identifies a mechanism by which mTORC1 modulates the interaction between ILC2s and neurons, highlighting a role for neuroimmune cross-talk in allergic asthma.

It is well established that ILC2s are activated by various stimuli, such as IL-33, IL-25, TSLP, and NMU[5,8,18,54–56]. Co-expression of the receptors recognizing these signals enables ILC2s to rapidly produce type 2 cytokines[7,10]. But how ILC2s integrate these tissue-derived signals and drive the pathogenic activation of ILC2s are unclear. Our work identified mTORC1 as a key regulator of ILC2 activation in allergic asthma. The findings that both IL-33 and IL-25 were elevated in allergic asthma and activated mTORC1 pathway in ILC2s[34–36] support that ILC2s integrate epithelial cytokines through mTORC1. Although NMU did not activate mTORC1, mTORC1 induced NMUR1 expression in ILC2s, leading to enhanced ILC2 activation in response to NMU. These results support the notion that mTORC1 promotes the cell interaction between neurons and ILC2s. Coupling epithelial signal and neuronal signal through mTORC1 to modulate ILC2 responses provides an efficient way to integrate multi-tissue responses to allergen challenge.

As a metabolic checkpoint kinase, mTORC1 is essential to control cell metabolism and growth by integrating exogenous growth factors, cytokines, and nutrients[25,26]. It has been shown that mTORC1 can

regulate T cell and ILC3 immune function and cell metabolism[29,31,33]. As expected, mTORC1 affected glucose metabolism in ILC2s, as indicted by decreased glycolysis and oxidative phosphorylation and reduced glucose uptake in Raptor-deficient ILC2s. The decreased cell proliferation and reduced acetyl-CoA level in Raptor-deficient ILC2s might be due to the disrupted glucose metabolism. In addition to glucose metabolism, one recent study has shown that mTORC1 regulates lipid

metabolism in activated ILC2s by controlling the expression of Pparg and Dgat1[36]. Consistent with these findings, we found Raptor-deficient ILC2s had decreased lipid uptake as well. Furthermore, mTORC1 regulated the immune function of ILC2s, as shown by diminished type 2 cytokines in Raptor-deficient ILC2s. The impaired ILC2 function has been linked to decreased acetyl-CoA, which led to less histone H3 acetylation and reduced NMUR1 expression. However, overexpression

Fig. 5 | mTORC1 promotes ILC2 activation partly through upregulation of NMUR1. a, b Lung ILC2s sorted from R5/+ (Control) and R5/+ Rptor[f/f] (KO) mice were infected with retrovirus expressing MIG or MIG-NMUR1. GFP^{+} infected cells were purified and cultured for 24 h in the presence of IL-7 (10 ng/ml) and NMU (10 ng/ml). The concentrations of IL-5 (a) and IL-13 (b) in culture supernatant were analyzed by ELISA (n = 13, 12, 9 from left to right). **c–e** Wild-type mice were challenged with papain intranasally. Lung tissues were collected at the indicated time points. **c** mRNA expression of Neuropeptide NMU in lung tissue (n = 3). **d** Quantification of NMU in the plasma of mice using ELISA (n = 4). **e** Relative mean fluorescence intensity (MFI) of NMUR1 in ILC2s (n = 4). **f–j** Lung ILC2s sorted from R5/+ (Control) and R5/+ Rptor[f/f] (KO) mice were infected with retrovirus expressing MIG or MIG-NMUR1. GFP^{+} infected cells were transferred to Rag2^{−/−}Il2rg^{−/−} mice, which were challenged with papain subsequently. The lungs were harvested and analyzed on day 7 (n = 5). **f** The number of ILC2s in the lungs. **g, h** Frequency and absolute counts of IL-5^{+} ILC2s (g) and IL-13^{+} ILC2s (h). **i** Absolute counts of lung eosinophils. **j** Alcian Blue–Periodic Acid–Schiff (AB-PAS) staining of lung sections and histological quantification of AB-PAS[+] area by ImageJ. Scale bars, 50 μm. Each symbol represents an individual mouse (**a–j**). Data were pooled from two independent experiments, shown as mean ± SEM. Statistical significance was tested by one-way ANOVA followed by Tukey's multiple comparisons test in (**a–j**). p-values are shown on the graphs, and p-values < 0.0001 are reported as such. Source data are provided as a Source Data file.

of NMUR1 in Raptor-deficient ILC2s only partially restored ILC2 effector function. These data suggest that other NMUR1-independent regulatory mechanisms exist. Whether lipid metabolism or transcriptional control mediated by mTORC1 are involved requires further investigation.

Previous studies have shown that rapamycin can suppress IL-33 induced ILC2 activation both in vitro and in vivo[34,50]. But the molecular mechanisms of mTORC1 regulating ILC2 function remain unknown. In our study, we identify mTORC1 signaling as a cause of pathogenic ILC2 activation in protease- and HDM-induced allergic asthma models. Moreover, we reveal that mTORC1 regulates NMUR1 expression to coordinate neuron-ILC2 crosstalk for ILC2 optimal activation through metabolic-epigenetic regulatory mechanisms. Therefore, inhibition of mTORC1 or HAT activity could suppress ILC2 activation and reduce allergic airway inflammation. Notably, we demonstrate that the therapeutic benefit of rapamycin in asthma is dependent on ILC2s, as evidenced by the loss of therapeutic effect of rapamycin in ILC2-deficient mice. Our study identifies mTORC1 as a critical regulator of ILC2 activation in allergic asthma and uncovers the mechanisms underlying the therapeutic action of rapamycin in asthma.

Methods
Mice
All mice used in this study were on the C57BL/6 J genetic background. Il5[tm1.1(icre)Lky/J] (R5/+) mice (Stock number: 030926), Rptor[tm1.1Dmsa/J](Rptor[f/f]) (Stock number: 013188), Rag1^{−/−} mice (Stock number: 002216), and ROSA26iDTR mice (Stock number: 007900) were purchased from the Jackson Laboratory. Rag2^{−/−}Il2rg^{−/−} mice (Stock number: 4111) were purchased from Taconic Biosciences. Nmur1-P2A-icre-P2A-tdTomato (Nmur1[iCre-TdT]) mice were generously provided by Dr. Heping Xu at Westlake University[42]. R5/+ and Rptor[f/f] mice were crossed to generate an R5/+ Rptor[f/f] strain. Nmur1[iCre-TdT] and Rptor[f/f] mice were crossed to generate a Nmur1[iCre-TdT] Rptor[f/f] strain. Nmur1[iCre-TdT] and ROSA26iDTR mice were crossed to generate a Nmur1[iCre-TdT] DTR[f/+] strain. Mice used in this study were age-matched (6–10 weeks) and sex-matched (male and female). Mice were maintained at accredited animal facilities under specific pathogen-free conditions on a strict 12 h day-night cycle with a regular chow diet at 20–24 °C and 45–65% humidity. All animals were euthanized by intraperitoneal injection of an overdose of sodium pentobarbital (150 mg/kg). All animal experiments were performed in compliance with the Guide for the Care and Use of Laboratory Animals, approved by Shanghai Jiao Tong University School of Medicine Institutional Animal Care and Use Committees (IACUC) (Project JUMC2023-110-A).

Allergen-induced airway inflammation models
Mice were anesthetized with isoflurane gas first. For the papain-induced model, mice were challenged intranasally with papain (50 μg per mouse) daily for five consecutive days. Bronchoalveolar lavage fluid (BALF) and lungs were collected on day 6 or at the indicated time points. For rapamycin treatment, mice were intraperitoneally injected with rapamycin (4 mg/kg body weight) for 5 days during papain

challenge. For anti-Thy1.2 antibody treatment, Rag1^{−/−} mice were intraperitoneally injected with 200 μg of anti-Thy1.2 or IgG1 isotype control antibody every 3 days for 3 weeks prior to papain administration. For HATi-A-485 treatment, mice were intraperitoneally injected with HATi (50 mg/kg body weight) for 5 days during papain challenge. For diphtheria toxin treatment, Nmur1[iCre-TdT] DTR[f/+] mice were intraperitoneally injected with diphtheria toxin (400 ng/day) for 2 days before papain administration. For HDM-induced allergic asthma. Mice were sensitized intranasally with 1 μg HDM extract at day 0 for primary immunizations and then intranasally boosted on 5 consecutive days between day 6 and day 10 with 10 μg HDM extract. Mice were sacrificed and analyzed on day 14. For Alternaria alternata-induced allergic asthma. Mice were administered intranasally with Alternaria alternata (25 μg per mouse, Greer Labs) for 4 consecutive days. Tissues were harvested 24 hours after the last challenge. For NMU-induced inflammation. Mice were administered NMU (20 μg per mouse) intranasally for five consecutive days, and mice were sacrificed and analyzed on day 8.
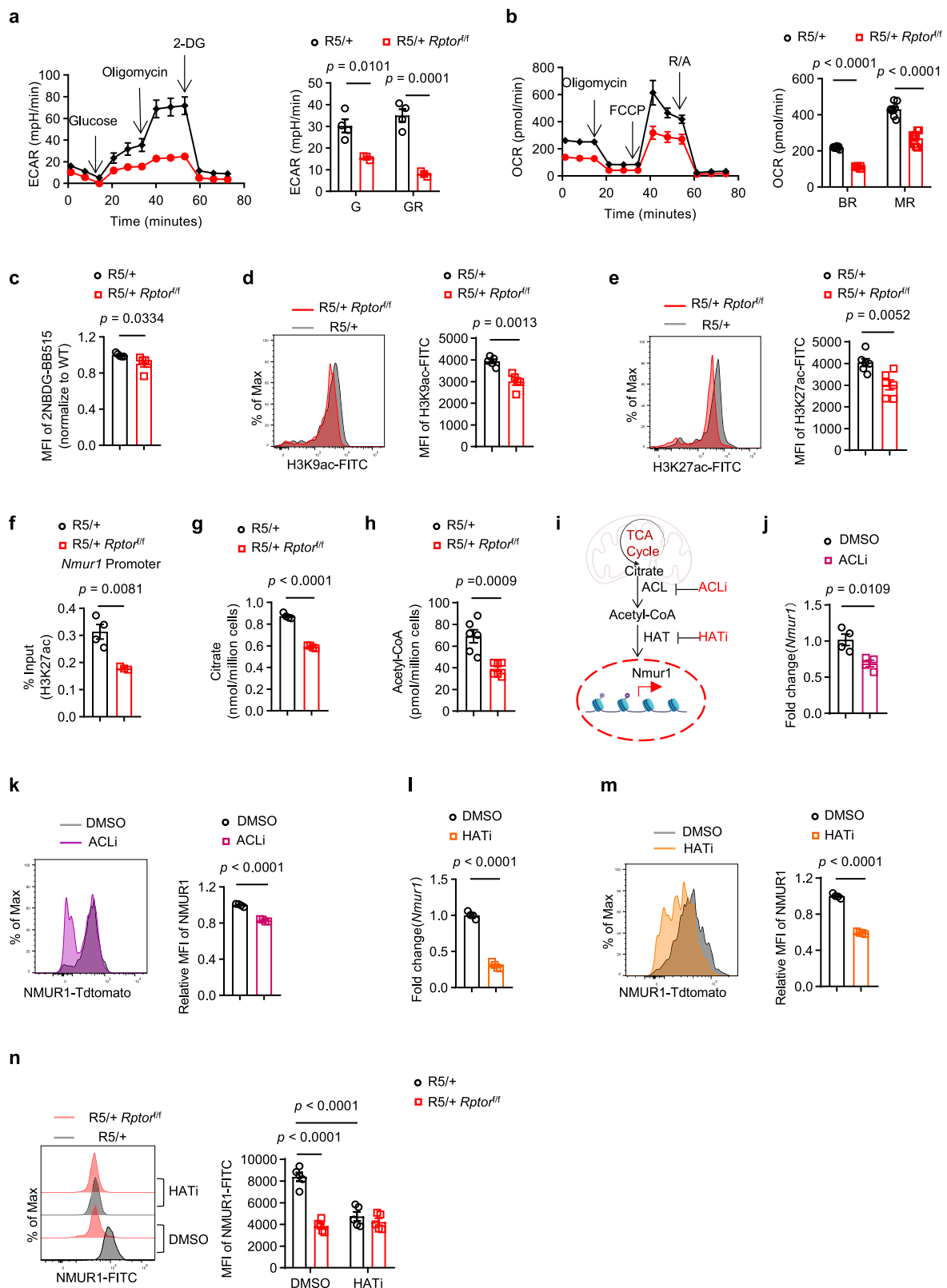
Preparation of cell suspensions from tissues
Bronchoalveolar lavage fluid (BALF) was collected with a 1 mL syringe with a 22-G needle and inserted into a small incision in the exposed mouse trachea, and cold PBS was instilled and withdrawn three times[57]. BALF was then centrifuged to spin down the cells for flow cytometry. The cell-free supernatants were stored at −80 °C for later cytokine analysis. To isolate immune cells from lung tissues, the lung was cut into pieces and digested in 5 ml of RPMI 1640 medium (Thermo Fisher Scientific) containing collagenase VIII (200 U/mL, Sigma-Aldrich), 10% FBS (Gibco), and DNase I (750 μg/mL, Sigma-Aldrich) at 37 °C for 1 hour. The digested tissues were filtered through 70 μm cell strainer. Mononuclear cells were collected from the interphase of a 30% and 70% Percoll (GE Healthcare) gradient following centrifugation at 1258 × g for 20 min at room temperature.

For isolation of immune cells from the large intestine and small intestine, fat and Peyer's patches were removed, and the intestines were cut into pieces and washed in PBS. Intestines were incubated and shaken at 250 r.p.m. in PBS containing 1 mM dithiothreitol (Sigma) and 30 mM EDTA (Sangon Biotech) for 10 min and then in PBS containing 30 mM EDTA (Sangon Biotech) for 10 min. Then the tissues were washed with RPMI 1640 medium for 2 min and digested in RPMI 1640 medium containing 10% FBS (Gibco), DNase I (150 μg/ml) and collagenase VIII (150 U/ml) at 37 °C for 1.5 h. Intestinal mononuclear cells were collected from the interphase of a 40% and 80% Percoll (GE Healthcare) gradients after centrifugation at 1258 × g for 20 min at room temperature.

For isolation of stromal vascular fraction (SVF) cells from adipose tissue, epididymal white adipose tissue was collected, cut into pieces, and digested in 4 ml of HBSS buffer (Gibco) containing collagenase I (200 U/mL, Sigma-Aldrich) at 37 °C with shaking for 40 min. The digested tissues were spun at 400 × g for 5 min at room temperature to obtain cell pellets.

Bone marrow cells were processed by flushing the femur and tibia with a syringe. Red blood cells were lysed with ACK buffer (Gibco) and

centrifuged at $400 \times g$ for 5 min. Cells were resuspended in FACS buffer (PBS + 2% FBS + 1 mM EDTA) for flow cytometry.

Human PBMCs collection

Human peripheral blood samples were collected from Shanghai Chest Hospital, Shanghai Jiaotong University School of Medicine. Asthma diagnosis was confirmed according to the Global Initiative for Asthma (GINA) criteria, based on characteristic respiratory symptoms and variable airflow limitation. Lung function was assessed, and parameters, including pre-bronchodilator FEV1% predicted, FEV1/FVC ratio, were documented. Total IgE levels (≥60 kU/L, ImmunoCap, Pharmacia Diagnostics AB, Uppsala, Sweden) were also measured. Patients experiencing acute exacerbations, with autoimmune or infectious diseases, or with recent (within 1 month) systemic glucocorticoid or

Fig. 6 | mTORC1 induces NMUR1 expression through an epigenetic mechanism.
a, **b** Seahorse analysis of the extracellular acidification rate (ECAR) (**a**) ($n = 4$ for R5/+, $n = 3$ for R5/+ $Rptor^{f/f}$) and oxygen consumption rate (OCR) (**b**) ($n = 8$) in lung ILC2s. G, glycolysis; GR, glycolytic reserve; BR, basal respiration; SRC, spare respiratory capacity. **c** Mean fluorescence intensity (MFI) of 2-(N-[7-nitrobenz-2-oxa-1,3-diazol-4-yl] amino) −2-deoxyglucose (2-NBDG) in lung ILC2s ($n = 5$). **d**, **e** MFI of global histone 3 (H3) acetylation at lysins K9 (H3K9ac, $n = 5$) (**d**) and K27 (H3k27ac, $n = 6$) (**e**). **f** Quantification of H3K27 acetylation at the NMUR1 promoter by ChIP-qPCR in ILC2 from R5/+ and R5/+ $Rptor^{f/f}$ mice ($n = 4$ for R5/+, $n = 3$ for R5/+ $Rptor^{f/f}$). **g** Analysis of citrate concentrations in ILC2s from R5/+ and R5/+ $Rptor^{f/f}$ mice ($n = 4$). **h**, Level of Acetyl-CoA in ILC2s from R5/+ and R5/+ $Rptor^{f/f}$ mice ($n = 6$). **i** Schematic diagram, schematic created in part with BioRender. Shen, L. (2025) https://BioRender.com/udwx3db. **j–m** Sorted ILC2s were treated with ATP citrate lyase inhibitor (ACLi) (30 μM) (**j**, **k**) or Histone Acetyltransferase inhibitor (HATi) (1 μM) (**l**, **m**) for 48 h. mRNA expression of *Nmur1* (**j**, **l**) and relative MFI of NMUR1-Tdtomato (**k**, **m**) was determined in ILC2s ($n = 4$). **n**, Sorted lung ILC2s from R5/+ and R5/+ $Rptor^{f/f}$ mice were treated with HATi (1 μM) for 48 h. Expression of NMUR1 in ILC2s was determined by flow cytometry ($n = 5$). Data were pooled from two independent experiments (**a–h**, **n**), and data are representative of two (**j–m**) independent experiments shown as mean ± SEM. Statistical significance was tested by two-tailed unpaired Student's *t* test in (**a–m**) or two-way ANOVA followed by Tukey's multiple comparisons test in (n). *p*-values are shown on the graphs, and *p*-values < 0.0001 are reported as such. Source data are provided as a Source Data file.

immunosuppressant treatment were excluded. Participant characteristics are detailed in supplementary Table 1. Ethical approval was provided by the Shanghai Chest Hospital Ethics Committee (accession number: KS(Y)24267). All of the patients provided informed consent before use during the study. Peripheral blood mononuclear cells (PBMCs) were isolated using Ficoll-Paque PLUS (GE Healthcare) by centrifugation at $400 \times g$ for 30 min at room temperature. The isolated PBMCs were washed and resuspended in PBS containing 2% fetal bovine serum (FBS). Human ILC2s were defined as lin⁻ (CD1a⁻CD3⁻CD5⁻CD11b⁻CD11c⁻CD14⁻CD15⁻CD16⁻CD19⁻FcεR1⁻) CD45⁺CD127⁺CRTH2⁺ live cells.

Flow cytometry and cell sorting
Dead cells were identified with fixable viability stain 570, fixable viability stain 510, or fixable viability stain 520 (BD Biosciences). Fc receptors were blocked with CD16/32 antibody (Biolegend) for 5 min at room temperature before surface staining. For surface staining, cells were stained with antibody cocktails in 100 μL of FACS buffer (BD Biosciences) at 4 °C in the dark for 30 min. For transcription factor staining and Ki67 proliferation assays, cells were fixed and permeabilized with Foxp3 fixation/permeabilized kit (Thermo Fisher Scientific) at 4 °C for 45 min, followed by staining in 100 μL of 1× permeabilized buffer containing antibody at 4 °C for 45 min. For cytokine staining, cells were stimulated with PMA (50 ng/mL, Sigma-Aldrich), ionomycin (500 ng/mL, Sigma-Aldrich), and brefeldin A (2 μg/mL, Sigma-Aldrich) for 4 hours before staining. For phosphorylation staining, cells were fixed by Phosflow™ Fixation Buffer I (BD Biosciences) for 30 min at room temperature, stained with phosphorylated antibody for 30 min at room temperature, followed by secondary antibody staining for 30 min at room temperature. For apoptosis assay, cells are fixed and permeabilized with BD Cytofix/Cytoperm kit (BD Biosciences) at 4 °C for 45 min, then stained with caspase-3 antibody in 100 μL of 1 × BD Perm/Wash buffer at 4 °C for 45 min in the dark. For NMUR1 staining, cells were fixed with 4% PFA at 4 °C for 20 min, permeabilized with 0.1% Triton X-100 at 4 °C for 15 min, then stained with NMUR1 antibody for 45 min at 4 °C, followed by secondary antibody for 45 min at 4 °C. To assess histone modifications, cells were fixed with the Foxp3/TF staining buffer set (eBioscience) for 30 min and stained intranuclearly with antibodies for 30 min in permeabilization buffer (eBioscience). After washing, anti-histone antibodies were detected using a donkey polyclonal anti-rabbit IgG secondary antibody conjugated to Alexa Fluor 488 (Invitrogen) for 30 min at room temperature. For cell sorting, lung ILC2s were sorted as lin⁻(CD3⁻B220⁻GR1⁻CD11b⁻CD11c⁻) CD45⁺CD25⁺ST2⁺ live cells.

ILC2 culture in vitro
Sorted ILC2s were cultured in complete RPMI 1640 medium containing 10% FBS (Gibco), 2 mM glutamine (Gibco), 50 μM β-mercaptoethanol, 333 μ/mL penicillin (Gibco), 333 μg/mL streptomycin (Gibco) and 10 ng/mL IL-7 (Peprotech) in 96-well flat-bottom plate. For cell proliferation or IL-33 stimulation experiments, sorted ILC2s were cultured

with IL-33 (10 ng/mL) under the specified experimental conditions. For the NMU stimulation experiment, sorted ILC2s were cultured with NMU (10 ng/mL) for 24 h for cytokine measurement. For other experiments, sorted ILC2s were cultured for 24 h or 48 h in the presence of rapamycin (0.5 μM) or the p300/CBP HAT domain inhibitor A 485 (1 μM), ATP citrate lyase inhibitor ACLi (30 μM).

Metabolic assays
For glucose and fatty acid uptake assay, sorted ILC2s were incubated in RPMI 1640 complete medium containing 100 μM of 2-(N-[7-nitrobenz-2-oxa-1,3-diazol-4-yl] amino) −2-deoxyglucose (2-NBDG, Invitrogen) or 1 mM of BODIPY FLC16 probe (Invitrogen) for 30 min at 37 °C. Cells were then washed with cold PBS and stained with surface markers. For the seahorse cellular metabolic assay, mice were injected intraperitoneally (i.p.) with 500 ng of IL-33 for 5 consecutive days to expand ILC2 compartments. On day 6, lung ILC2s were sorted and cultured for another 3 days in a complete medium for proliferation. Cells were then plated at 150,000 cells per well, and OCR and ECAR were measured by the Mito stress test kit (Agilent) according to the manufacturer's protocol. Measurements were taken on an XF96 extracellular flux analyzer (Seahorse Bioscience).

For measurement of cytosolic acetyl-CoA, sorted lung ILC2s were treated with lysis buffer (1% Triton X-100, 20 mM Tris-HCl, pH = 7.4, 150 mM NaCl) on ice for 10 min. The lysates were centrifuged at 20, $000 \times g$ for 10 min at 4 °C, the pellets (nuclei and heavy membrane) were discarded, and the supernatants were collected for acetyl-CoA measurement with an Acetyl-CoA Assay Kit (Sigma).
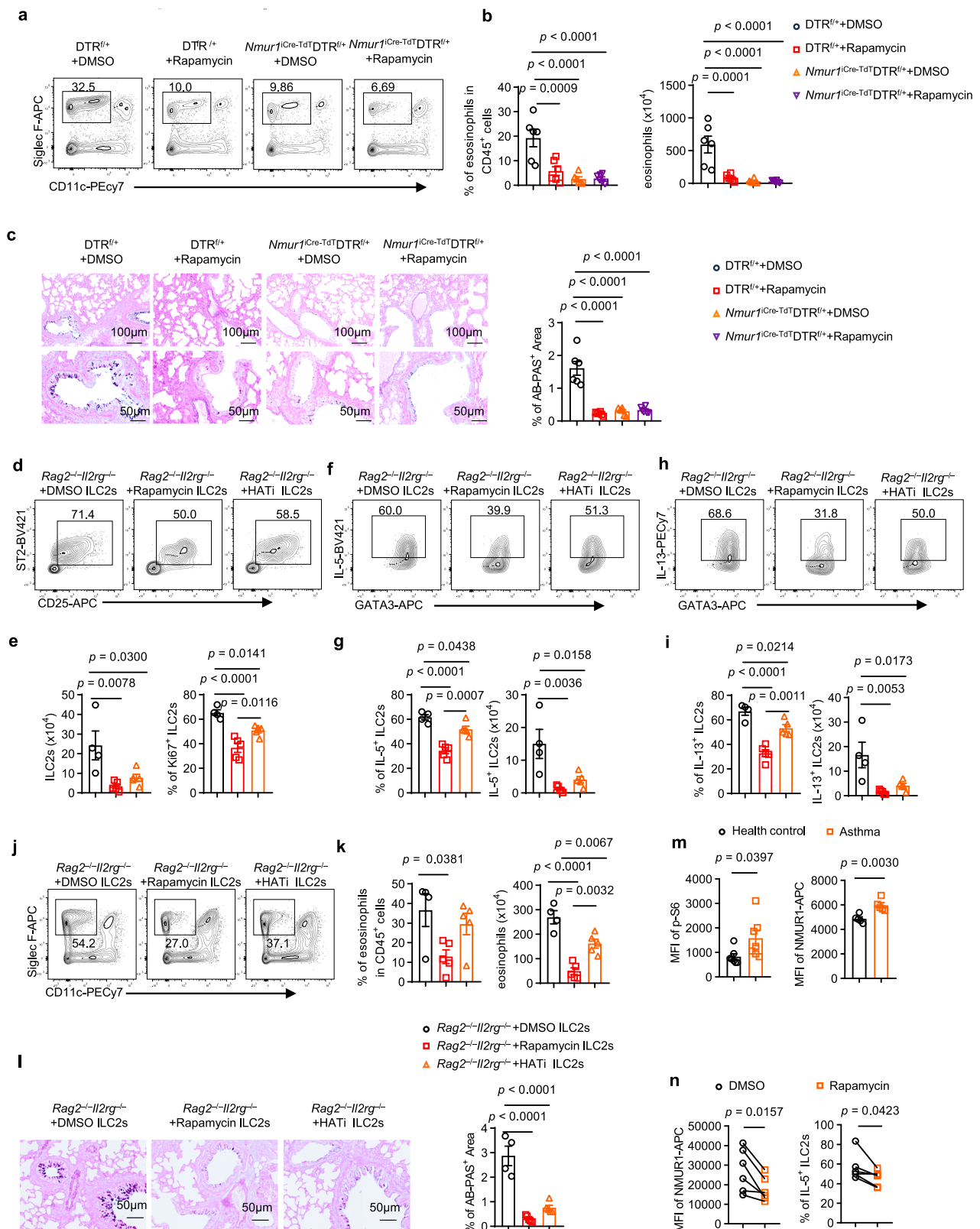
For the measurement of Citrate, the concentration of citrate of ILC2s was determined using a Citrate Assay Kit (Abcam) according to the manufacturer's instructions.

Retroviral infection of ILC2s
MSCV-IRES-GFP (MIG) was kindly provided by Dr. Ju Qiu (Shanghai Institute of Nutrition and Health). Mouse *Nmur1* cDNA was cloned into the retroviral vector MSCV-IRES-GFP (MIG). Phoenix cells were transfected with the retroviral plasmid and packaging plasmid 10A1 using polyethyleneimine (PEI, Polysciences). Viral supernatants were collected after transfection. For retroviral infection of ILC2s (using MIG or MIG-NMUR1), purified lung ILC2s from R5/+ or R5/+ $Rptor^{f/f}$ mice were expanded in vitro with IL-7 and IL-33 for 5 days. On day 5, ILC2s were plated in 96-well flat-bottom plates in 200 μL of virus supernatant containing 8 μg/mL polybrene (Sigma-Aldrich), IL-7 (10 ng/mL), and IL-33 (10 ng/mL). The plates were spun at $1258 \times g$ for 2 h at 30 °C and placed in 5% CO_2 in incubator for additional 2 h. Virus supernatants were then replaced with complete medium containing IL-33. The infected GFP + cells were sorted 72 h after viral infection and used for subsequent studies.

Adoptive transfer
For assess cell-intrinsic ILC2 functions, R5/+ and R5/+ $Rptor^{f/f}$ (KO) mice were injected with 500 ng of IL-33 for 5 consecutive days to expand ILC2 compartments. Then, 2×10^5 ILC2s sorted from R5/+ and

R5/+ *Rptor*^f/f mice were transferred intravenously into *Rag2*^−/−*Il2rg*^−/− mice. For rapamycin or HATi treatment experiments, wild-type mice were injected intraperitoneally with 500 ng IL-33 daily for 5 consecutive days to expand ILC2s. And 2 × 10⁵ ILC2s were then sorted from WT mice, pretreated with rapamycin, HATi or DMSO control for 48 h, and adoptively transferred intravenously into *Rag2*^−/−*Il2rg*^−/− mice.

Cytokine detection

The concentrations of IL-5 and IL-13 in BALF or cell culture supernatants were measured by an ELISA Kit (Thermo Fisher Scientific). Blood samples were collected and serum was separated by centrifugation at 1000 × g for 15 min. The NMU level in the serum was measured with the Mouse Neuromedin-U (NMU) ELISA Kit (MOEB1702, Assay Gene).

Fig. 7 | Blockade of mTORC1-NMUR1 pathway in ILC2s ameliorates allergic asthma. a–c DTR$^{f/+}$ and $Nmur1^{iCre\text{-}TdT}$DTR$^{f/+}$ mice were treated with diphtheria toxin for 3 days. Then the mice were challenged with papain and treated with rapamycin (4 mg/kg body weight) intraperitoneally for five days. Lung tissues were collected and analyzed on day 6 ($n = 6$). **a, b** Frequency and absolute numbers of eosinophils in the lung tissue. **c** Alcian Blue–Periodic Acid–Schiff (AB-PAS) staining of the lung sections. Quantification of AB-PAS$^+$ area by ImageJ. Scale bars, 100 μm or 50 μm. **d–l** WT ILC2s were pretreated with rapamycin, histone acetyltransferase inhibitor (HATi), or DMSO and adoptively transferred into $Rag2^{-/-}Il2rg^{-/-}$ mice. Recipient mice were challenged with papain, and lung tissues were collected and analyzed on day 7 ($n = 4, 5, 5$ from left to right). **d, e** The number of ILC2s and frequency of Ki67$^+$ILC2s in the lungs. **f, g** Frequency and absolute counts of IL-5$^+$ ILC2s. **h, i**

Frequency and absolute counts of IL-13$^+$ ILC2s. **j, k** Frequency and absolute numbers of eosinophils in the lung tissue. **l** AB-PAS staining of the lung sections. Quantification of AB-PAS$^+$ area by ImageJ. Scale bars, 50 μm. **m** Mean fluorescence intensity (MFI) of p-S6 ($n = 7$) and NMUR1 ($n = 5$) on peripheral blood ILC2s from health controls and asthma patients. **n** PBMCs from asthma patients were treated with rapamycin for 24 h. NMUR1 expression and IL-5 production were determined ($n = 6$). Data were pooled from two independent experiments (**a–l**), shown as mean ± SEM. Statistical significance was determined by one-way ANOVA followed by Tukey's multiple comparisons test in (**b, c, e, g, i, k** and **l**), two-tailed unpaired Student's t test in (**m**), two-tailed paired Student's t test in (**n**). p-values are shown on the graphs, and p-values < 0.0001 are reported as such. Source data are provided as a Source Data file.

Quantitative real-time PCR
RNA was extracted from sorted cells using Trizol reagent (Invitrogen). cDNA was transcribed with PrimeScript RT Master Kit (Takara). Real-time quantitative PCR (qPCR) was performed using SYBR Green qPCR Master Mix (Low ROX) (Selleck), and reactions were run with the QuantStudio 7 (Thermo Fisher Scientific). The results are displayed as relative expression values normalized to *Actb* or *Hprt*. The primers used for quantitative qPCR are listed in Supplementary Table 2.

ChIP-qPCR
R5/+ and R5/+ *Rptor*$^{f/f}$ (KO) mice were injected with 500 ng of IL-33 for 5 consecutive days, and sort-purified ILC2 cultured for five days in vitro to expand ILC2 compartments. Then, Chromatin immunoprecipitations (ChIP) were then performed using the SimpleChIP Enzymatic Chromatin IP Kit (Cell Signaling) following the manufacturer's instructions. The relative abundance of precipitated DNA fragments was analyzed by qPCR with SimpleChIP Universal qPCR Master Mix (Cell Signaling). The following primers were used for qPCR are listed in supplementary Table 3.

RNA-seq
Lung ILC2s were sorted from mice treated with PBS or the protease allergen papain, or from R5/+ and R5/+ *Rptor*$^{f/f}$ (KO) mice after papain treatment. Total RNA was extracted from the sorted lung ILC2s using Trizol reagent. RNA quality was assessed with an Agilent Bioanalyzer 2100 (Agilent). High-quality full-length cDNA was synthesized with the SMART-Seq HT Kit (Takara Bio USA). Sequencing libraries were generated using the TruePrep DNA Library Prep Kit V2 for Illumina (Vazyme), following the manufacturer's protocol. The libraries were sequenced on the Illumina HiSeq X Ten system. Raw reads were aligned to the mouse reference genome (version mm10) using Hisat2 RNA-seq alignment software. Relative mRNA expression levels (FPKM) were quantified based on exon regions using Cufflinks and the mm10 genome annotation.

Immunoblot analysis
Sorted lung ILC2s (1×10^5 cells) were lysed in RIPA buffer (Beyotime) containing protein inhibitor (Thermo Fisher Scientific) and phosphatase inhibitor on ice for 30 min. The supernatants were mixed with SDS-PAGE loading buffer (Beyotime) and incubated at 100 °C for 5 min. Proteins were separated on 12% Tris-Glycine gels and transferred onto Immobilon-P transfer membranes (Merck Millipore). The membrane was blocked in 5% nonfat dried milk for 2 h and incubated overnight with the primary antibody at 4 °C. The corresponding HRP-conjugated secondary antibodies were added to the membranes for 2 h at room temperature. Detection was performed with ECL western blotting detection reagents (Millipore) using Amersham Imager 600.

Histologic analysis
Left lung tissues from mice were immediately fixed in 4% paraformaldehyde. The tissues were then embedded in paraffin, and 7 μm

sections were cut at the largest cross-section. Sections were stained with hematoxylin and eosin (H&E) or Alcian Blue–Periodic Acid–Schiff (AB-PAS) to assess mucin production and then were examined by light microscopy.

Immunofluorescence microscopy
For NMUR1 staining, sorted lung ILC2s from R5/+ and R5/+ *Rptor*$^{f/f}$ mice were transferred to adhesion microscope slides (Citotest) using CYTOSPIN 4 (Thermo Scientific). Cells were fixed with 4% PFA in PBS for 10 min, permeabilized with 0.1% Triton X-100, and blocked with 10% serum (45 min at room temperature), incubated with rabbit anti-NMUR1 polyclonal antibody at 4 °C overnight, followed by staining with Alexa Fluor 488-conjugated anti-rabbit IgG (Invitrogen, 1:500) for 1 h at room temperature. The Slides were mounted with DAPI Fluoromount-GTM (Yeasen) and analyzed with confocal microscopy (LEICA DM6B). Lungs were collected from $Nmur1^{iCre\text{-}TdT}$ reporter mice infused with 650 μL of UltraPure low-melting-point agarose (1.0% in PBS, pre-warmed to 39 °C; Invitrogen, Thermo Fisher Scientific, 16520-050) via the trachea. Tissues were collected and fixed overnight in 4% paraformaldehyde (PFA; ServiceBio, G1101), followed by sequential dehydration in 15% and 30% sucrose and embedding in OCT compound (Sakura Finetek, 4583). Sections (60 μm) were cut on a Leica cryostat and permeabilized with 0.1% Triton X-100 for 2 h. After blocking with 4% BSA (Kingmorn, KS1090) for 2 h at room temperature, sections were incubated with primary antibodies diluted in PBS containing 0.2% Tween-20 at 4 °C in a dark, humidified chamber. The following antibody was used: β-tubulin III (Cell Signaling Technology, 5568S), Alexa FluorTM 750 (Invitrogen, A21039). Slides were mounted with antifade mounting medium (Yeasen) and imaged using an Olympus FluoView FV4000 confocal microscope equipped with a UPlanSApo ×20/0.75 objective (Olympus).

Statistical analysis
Statistical analyses were performed using GraphPad Prism 8.0.1. Unless otherwise noted, statistical significance was determined by the two-tailed unpaired or paired Student's t test for comparing two groups, by one-way or two-way analysis of variance analysis (ANOVA) on individual biological samples. Detailed information on the statistical analyses is included in the figure legends. Data from the experiments are presented as mean values ± SEM. p-values are noted in each figure.

Reporting summary
Further information on research design is available in the Nature Portfolio Reporting Summary linked to this article.

Data availability
The ILC2 bulk RNA-seq dataset generated in this study have been deposited in the GEO database under accession codes GSE272521 and GSE272716. The raw reads of RNA-seq were aligned to the mouse reference genome (version mm10). All other data generated in this

study are available in the article and supplementary files. Source data are provided in this paper.

References

1. Porsbjerg, C., Melén, E., Lehtimäki, L. & Shaw, D. Asthma. *Lancet* **401**, 858–873 (2023).
2. Paul, W. E. & Zhu, J. How are T(H)2-type immune responses initiated and amplified?. *Nat. Rev. Immunol.* **10**, 225–235 (2010).
3. Halim, T. Y., Krauss, R. H., Sun, A. C. & Takei, F. Lung natural helper cells are a critical source of Th2 cell-type cytokines in protease allergen-induced airway inflammation. *Immunity* **36**, 451–463 (2012).
4. Peebles, R. S. Jr & Aronica, M. A. Proinflammatory pathways in the pathogenesis of asthma. *Clin. Chest Med.* **40**, 29–50 (2019).
5. Halim, T. Y. et al. Group 2 innate lymphoid cells are critical for the initiation of adaptive T helper 2 cell-mediated allergic lung inflammation. *Immunity* **40**, 425–435 (2014).
6. Olguín-Martínez, E., Ruiz-Medina, B. E. & Licona-Limón, P. Tissue-specific molecular markers and heterogeneity in type 2 innate lymphoid cells. *Front. Immunol.* **12**, 757967 (2021).
7. Schuijs, M. J. & Halim, T. Y. F. Group 2 innate lymphocytes at the interface between innate and adaptive immunity. *Ann. N. Y Acad. Sci.* **1417**, 87–103 (2018).
8. Kim, B. S. et al. TSLP elicits IL-33-independent innate lymphoid cell responses to promote skin inflammation. *Sci. Transl. Med.* **5**, 170ra116 (2013).
9. Cording, S., Medvedovic, J., Aychek, T. & Eberl, G. Innate lymphoid cells in defense, immunopathology and immunotherapy. *Nat. Immunol.* **17**, 755–757 (2016).
10. Vivier, E. et al. Innate lymphoid cells: 10 years on. *Cell* **174**, 1054–1066 (2018).
11. Talbot, S. et al. Silencing nociceptor neurons reduces allergic airway inflammation. *Neuron* **87**, 341–354 (2015).
12. Cao, Y. et al. Dopamine inhibits group 2 innate lymphoid cell-driven allergic lung inflammation by dampening mitochondrial activity. *Immunity* **56**, 320–335 (2023).
13. Cardoso, V. et al. Neuronal regulation of type 2 innate lymphoid cells via neuromedin U. *Nature* **549**, 277–281 (2017).
14. Klose, C. S. N. et al. The neuropeptide neuromedin U stimulates innate lymphoid cells and type 2 inflammation. *Nature* **549**, 282–286 (2017).
15. Moriyama, S. et al. β2-adrenergic receptor-mediated negative regulation of group 2 innate lymphoid cell responses. *Science* **359**, 1056–1061 (2018).
16. Nagashima, H. et al. Neuropeptide CGRP limits group 2 innate lymphoid cell responses and constrains type 2 inflammation. *Immunity* **51**, 682–695 (2019).
17. Tsou, A. M. et al. Neuropeptide regulation of non-redundant ILC2 responses at barrier surfaces. *Nature* **611**, 787–793 (2022).
18. Wallrapp, A. et al. The neuropeptide NMU amplifies ILC2-driven allergic lung inflammation. *Nature* **549**, 351–356 (2017).
19. Sui, P. et al. Pulmonary neuroendocrine cells amplify allergic asthma responses. *Science* **360**, https://doi.org/10.1126/science.aan8546 (2018).
20. Wallrapp, A. et al. Calcitonin gene-related peptide negatively regulates alarmin-driven type 2 innate lymphoid cell responses. *Immunity* **51**, 709–723 (2019).
21. Klein Wolterink, R. G. et al. Pulmonary innate lymphoid cells are major producers of IL-5 and IL-13 in murine models of allergic asthma. *Eur. J. Immunol.* **42**, 1106–1116 (2012).
22. Nussbaum, J. C. et al. Type 2 innate lymphoid cells control eosinophil homeostasis. *Nature* **502**, 245–248 (2013).
23. Zheng, H. et al. The role of type 2 innate lymphoid cells in allergic diseases. *Front. Immunol.* **12**, 586078 (2021).
24. Cosmi, L., Liotta, F., Maggi, L. & Annunziato, F. Role of type 2 innate lymphoid cells in allergic diseases. *Curr. Allergy Asthma Rep.* **17**, 66 (2017).
25. Ben-Sahra, I. & Manning, B. D. mTORC1 signaling and the metabolic control of cell growth. *Curr. Opin. Cell Biol.* **45**, 72–82 (2017).
26. Saxton, R. A. & Sabatini, D. M. mTOR Signaling in growth, metabolism, and disease. *Cell* **169**, 361–371 (2017).
27. Düvel, K. et al. Activation of a metabolic gene regulatory network downstream of mTOR complex 1. *Mol. Cell* **39**, 171–183 (2010).
28. Zeng, H. & Chi, H. mTOR signaling and transcriptional regulation in T lymphocytes. *Transcription* **5**, e28263 (2014).
29. Yang, K. et al. T cell exit from quiescence and differentiation into Th2 cells depend on Raptor-mTORC1-mediated metabolic reprogramming. *Immunity* **39**, 1043–1056 (2013).
30. Kidani, Y. et al. Sterol regulatory element-binding proteins are essential for the metabolic programming of effector T cells and adaptive immunity. *Nat. Immunol.* **14**, 489–499 (2013).
31. Shi, L. Z. et al. HIF1alpha-dependent glycolytic pathway orchestrates a metabolic checkpoint for the differentiation of TH17 and Treg cells. *J. Exp. Med.* **208**, 1367–1376 (2011).
32. Dang, E. V. et al. Control of T(H)17/T(reg) balance by hypoxia-inducible factor 1. *Cell* **146**, 772–784 (2011).
33. Di Luccia, B., Gilfillan, S., Cella, M., Colonna, M. & Huang, S. C. ILC3s integrate glycolysis and mitochondrial production of reactive oxygen species to fulfill activation demands. *J. Exp. Med.* **216**, 2231–2241 (2019).
34. Salmond, R. J. et al. IL-33 induces innate lymphoid cell-mediated airway inflammation by activating mammalian target of rapamycin. *J. Allergy Clin. Immunol.* **130**, 1159–1166.e1156 (2012).
35. Hodge, S. H. et al. Amino acid availability acts as a metabolic rheostat to determine the magnitude of ILC2 responses. *J. Exp. Med.* **220**, https://doi.org/10.1084/jem.20221073 (2023).
36. Karagiannis, F. et al. Lipid-droplet formation drives pathogenic group 2 innate lymphoid cells in airway inflammation. *Immunity* **52**, 620–634 (2020).
37. Kubo, M. Innate and adaptive type 2 immunity in lung allergic inflammation. *Immunol. Rev.* **278**, 162–172 (2017).
38. Neill, D. R. et al. Nuocytes represent a new innate effector leukocyte that mediates type-2 immunity. *Nature* **464**, 1367–1370 (2010).
39. Battaglioni, S., Benjamin, D., Wälchli, M., Maier, T. & Hall, M. N. mTOR substrate phosphorylation in growth control. *Cell* **185**, 1814–1836 (2022).
40. Foster, K. G. et al. Regulation of mTOR complex 1 (mTORC1) by raptor Ser863 and multisite phosphorylation. *J. Biol. Chem.* **285**, 80–94 (2010).
41. Snelgrove, R. J. et al. Alternaria-derived serine protease activity drives IL-33-mediated asthma exacerbations. *J. Allergy Clin. Immunol.* **134**, 583–592.e586 (2014).
42. Li, Y. et al. Neuromedin U programs eosinophils to promote mucosal immunity of the small intestine. *Science* **381**, 1189–1196 (2023).
43. Moriyama, M. et al. Presynaptic modulation by neuromedin U of sensory synaptic transmission in rat spinal dorsal horn neurones. *J. Physiol.* **559**, 707–713 (2004).
44. Kim, S. H. et al. Mapping of the sensory innervation of the mouse lung by specific vagal and dorsal root ganglion neuronal Subsets. *eNeuro* **9**, https://doi.org/10.1523/eneuro.0026-22.2022 (2022).
45. Peng, M. et al. Aerobic glycolysis promotes T helper 1 cell differentiation through an epigenetic mechanism. *Science* **354**, 481–484 (2016).
46. Lu, C. & Thompson, C. B. Metabolic regulation of epigenetics. *Cell Metab.* **16**, 9–17 (2012).
47. Wellen, K. E. et al. ATP-citrate lyase links cellular metabolism to histone acetylation. *Science* **324**, 1076–1080 (2009).

48. Takahashi, H., McCaffery, J. M., Irizarry, R. A. & Boeke, J. D. Nucleo-cytosolic acetyl-coenzyme a synthetase is required for histone acetylation and global transcription. *Mol. Cell* **23**, 207–217 (2006).

49. Mushaben, E. M., Kramer, E. L., Brandt, E. B., Khurana Hershey, G. K. & Le Cras, T. D. Rapamycin attenuates airway hyperreactivity, goblet cells, and IgE in experimental allergic asthma. *J. Immunol.* **187**, 5756–5763 (2011).

50. Boberg, E. et al. Rapamycin dampens inflammatory properties of bone marrow ILC2s in IL-33-induced eosinophilic airway inflammation. *Front. Immunol.* **13**, 915906 (2022).

51. Zhang, J. et al. Neuropilin-1 mediates lung tissue-specific control of ILC2 function in type 2 immunity. *Nat. Immunol.* **23**, 237–250 (2022).

52. Sun, J. et al. Metabolic regulator LKB1 controls adipose tissue ILC2 PD-1 expression and mitochondrial homeostasis to prevent insulin resistance. *Immunity* **57**, 1289–1305.e1289 (2024).

53. Yano, H. & Artis, D. Neuronal regulation of innate lymphoid cell responses. *Curr. Opin. Immunol.* **76**, 102205 (2022).

54. Toki, S. et al. TSLP and IL-33 reciprocally promote each other's lung protein expression and ILC2 receptor expression to enhance innate type-2 airway inflammation. *Allergy* **75**, 1606–1617 (2020).

55. Huang, Y. et al. IL-25-responsive, lineage-negative KLRG1(hi) cells are multipotential 'inflammatory' type 2 innate lymphoid cells. *Nat. Immunol.* **16**, 161–169 (2015).

56. von Moltke, J., Ji, M., Liang, H. E. & Locksley, R. M. Tuft-cell-derived IL-25 regulates an intestinal ILC2-epithelial response circuit. *Nature* **529**, 221–225 (2016).

57. Monticelli, L. A. et al. Innate lymphoid cells promote lung-tissue homeostasis after infection with influenza virus. *Nat. Immunol.* **12**, 1045–1054 (2011).

Acknowledgements

Author contributions

D.W. performed the experiments and analyzed the data. L.H., J.C., L.Z., J.X.Q., Y.C., and M.Z. performed the experiments. W.Z. and W.T. contributed to human samples collection. X.S., J.S., J.Q., W.Z. and W.T. contributed to the discussion. L.S. and D.W. wrote the manuscript. L.S. conceived, designed, and supervised the project.

Competing interests

The authors declare no competing interests.

Additional information

Supplementary information The online version contains Supplementary Material available at https://doi.org/10.1038/s41467-025-66683-y.

Correspondence and requests for materials should be addressed to Wei Tang, Wenyong Zhou or Lei Shen.

Peer review information *Nature Communications* thanks Damon Tumes and the other anonymous reviewer(s) for their contribution to the peer review of this work. A peer review file is available.

Reprints and permissions information is available at http://www.nature.com/reprints

Publisher's note Springer Nature remains neutral with regard to jurisdictional claims in published maps and institutional affiliations.